# Overvoltages due to Synchronous Tripping of Plug-in Electric-Vehicle Chargers Following Voltage Dips

Soumya Kundu, *Member, IEEE*, and Ian A. Hiskens, *Fellow, IEEE*

***Abstract*—Plug-in electric vehicle (PEV) charging equipment incorporates protection that ensures that grid disturbances do not damage the charger or vehicle. When the grid voltage sags below 80% of nominal, undervoltage protection is likely to disconnect the charging load from the grid. Most PEV charging will occur overnight, when non-PEV load is at a minimum. This paper argues that PEV voltage-sag response, when synchronized across large numbers of PEVs, could result in the loss of a significant proportion of the total load. It is shown that this load loss can lead to unacceptably high voltages once the initiating event has been cleared. This paper explores the nature of this voltage-rise phenomenon. Analysis tools are developed to assist in determining PEV loading conditions that demarcate acceptable postdisturbance voltage response from unacceptable outcomes. Two examples, based on standard distribution test systems, are used to illustrate PEV-induced overvoltage behavior, and demonstrate applications of the analysis tools.**

***Index Terms*—Distribution networks, overvoltages, plug-in electric vehicles, voltage sag.**

## I. Introduction

MANY MARKET research reports suggest that by 2020, vehicles that acquire energy from the grid, referred to generically as plug-in electric vehicles (PEVs), may well account for around 20% of total automobile sales in the U.S. [1], [2]. It is therefore reasonable to assume that a large number of households will have at least one PEV. In many cases, these vehicles will charge from residential distribution feeders. Vehicle charging rates vary over a wide range, with SAE Standard J1772 [3] defining level 1 charge rates up to 1.9 kW, and level 2 up to 19.8 kW. It is anticipated that charging rates of around 5 kW will be quite common [4]. To put this load in context, average household electricity consumption is around 1.3 kW [5]. Furthermore, it is likely that financial incentives will encourage charging overnight, when background non-PEV demand is less than average [6]. Therefore, it may be concluded that during overnight hours, PEV-charging load will contribute a significant proportion of the total demand on residential distribution feeders.

When electricity demand is composed of large numbers of similar devices, relatively benign events can synchronize their response, resulting in collective behavior that is potentially destabilizing. Such a situation arises with fault-induced delayed voltage recovery (FIDVR) [7], where a voltage sag leads to large numbers of residential air-conditioner compressors stalling [8]. The high current drawn by the stalled induction motors depresses voltages further, and a cascading form of voltage collapse may result. It is shown in this paper that if the penetration of PEV-charging load is sufficiently high, the synchronized tripping of PEV chargers may lead to unacceptably high voltages on distribution feeders.

The response of PEV chargers to power-quality events is governed by SAE Standard J2894 [9], which updates an earlier report from the Electric Power Research Institute (EPRI) [10]. As with FIDVR, the response of PEV chargers to low-voltage events is of particular interest. Two cases are covered in SAE J2894:

Case 1) Voltage sag: PEV chargers must remain energized if the supply voltage drops to 80% of nominal for up to 2 s.

Case 2) Momentary outage: PEV chargers must ride through a complete loss of voltage for up to 12 cycles.

Situations where voltages sag below 80%, but remain nonzero, are not explicitly covered by the standard.

Voltage sag events that affect the entire distribution feeders are relatively common. Such events play a fundamental role in FIDVR, which has been observed on numerous occasions [7]. Therefore, it may be assumed that distribution networks will experience voltage sags that are sufficient to cause large numbers of PEV chargers to trip. Following such trips, SAE J2894 recommends that restarting be delayed, in order to minimize the possibility of cold-load pickup. As noted earlier, the PEV-charging load could contribute a large proportion of the total load on a distribution feeder during overnight hours. Accordingly, a voltage sag that tripped PEV chargers would cause a significant reduction in the total load.[1] Upon recovery from the voltage sag, the feeder would experience much lighter load and, consequently, voltages would exceed their predisturbance values. Shunt capacitors, which are common on distribution feeders, would further contribute to this voltage rise. A large voltage increase, perhaps above 110% of nominal, could cause

Manuscript received January 05, 2013; revised June 10, 2013; accepted January 23, 2014. Date of publication April 15, 2014; date of current version May 20, 2014. This work was supported in part by the National Science Foundation through EFRI-RESIN under Grant 0835995 and in part by the Department of Energy through the Clean Energy Research Centre for Clean Vehicle Collaboration (CERC-CVC) under award number DE-PI0000012. Paper no. TPWRD-00025-2013.

The authors are with the Department of Electrical Engineering and Computer Science, University of Michigan, Ann Arbor, MI 48109 USA (e-mail: soumyak@umich.com; hiskens@umich.edu).

Color versions of one or more of the figures in this paper are available online at http://ieeexplore.ieee.org.

Digital Object Identifier 10.1109/TPWRD.2014.2311112

[1]Other electrical appliances would also be likely to trip [11], further exacerbating the load loss.

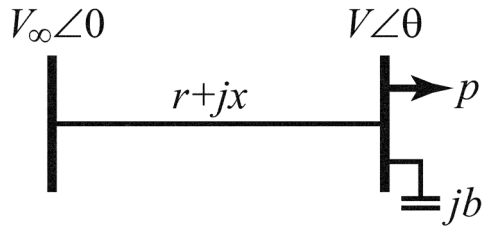


Fig. 1. Two-bus network.

other electrical equipment to trip. In fact, SAE J2894 allows PEV chargers to trip for voltages above 110% of nominal. The high voltages resulting from such a cascade could damage distribution equipment and the remaining load.

This overvoltage issue is explored in the remainder of this paper. Section II provides a motivating example. Section III establishes the network model that is used throughout the investigations, and draws together the assumptions regarding voltage control. Section IV describes the approach taken to investigate general distribution networks. Results are presented and discussed in Section V, and conclusions are provided in Section VI.

## II. Motivating Example

The simple two-bus network of Fig. 1 will be used to provide an initial illustration of voltage rise associated with PEV charger tripping. (Standard distribution feeder examples will be considered in Section V.) For clarity of presentation, the load in Fig. 1 has unity power factor. This simplification will be relaxed in the standard test cases discussed later. For this simple system, the relationship between active power load $p$, susceptance $b$, and load-bus voltage $V$ can be written

$$f(p,b,V;r,x,V_\infty) = \Big((1-bx)^2+(br)^2\Big)V^4 + \big(2pr-V_\infty^2\big)V^2 + p^2\big(r^2+x^2\big) = 0. \quad (1)$$

This relationship is shown graphically in Fig. 2, where each line corresponds to a particular value of voltage $V$, and can be thought of as a contour of the $(p,b,V)$-surface [12], [13].

It is assumed throughout this paper that voltages above 1.1 p.u. are unacceptable. Many devices will trip if voltages rise above this threshold, including PEV chargers [9]. As more loads trip, voltages will rise further, resulting in even higher overvoltages that could potentially cause widespread damage to electrical equipment.

For clarity of illustration, parameter values of $V_\infty = 1.0$ p.u., $r = 0.3$ p.u., and $x = 0.5$ p.u. will be used in this example, along with the base-case conditions $p = 0.5$ p.u. and $V = 1.0$ p.u. The capacitive susceptance required to achieve these loading conditions can be determined from (1) as $b = 0.46$ p.u. This base-case point is identified in Fig. 2. If the load power $p$ were to reduce, while holding susceptance $b$ constant, the operating point would move horizontally to the left, crossing contours of higher and higher voltage. For a sufficiently large loss of load $p$, the operating point would move to the unacceptable operating region where $V > 1.1$ p.u. By setting $V = 1.1$ p.u. in (1), the value of load at which voltage becomes unacceptable can be found to be $p = 0.364$ p.u. Therefore, in this example, if $(0.5 - 0.364)/0.5 = 27\%$ of the original load tripped, the voltage at the load bus would rise from 1.0 to 1.1 p.u.

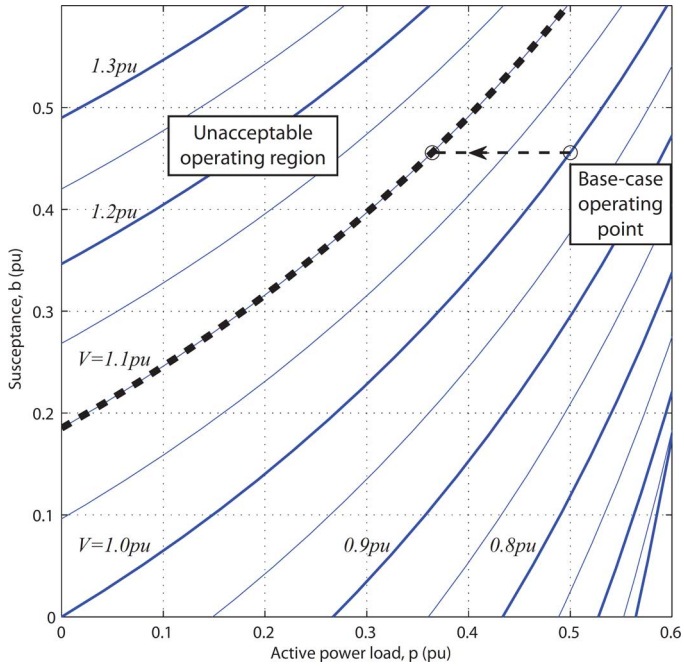


Fig. 2. Relationship between load power $p$, susceptance $b$, and voltage $V$.

## III. Basic Framework

### A. Generalized Network Description

In order to extend analysis from the two-bus case of Section II to realistic distribution feeders, the generic radial network structure shown in Fig. 3 will be adopted. Node 1 denotes the substation bus at the source of the feeder, while load nodes $2,\ldots,n$ are arranged so that the node number increases along paths from the substation to the end nodes. The set of feeder nodes is given by $\mathcal{N} = \{1,\ldots,n\}$. Let $\mathcal{C}$ be the set of all connections between nodes, so that $(i,j) \in \mathcal{C}$ if a physical connection exists between nodes $i$ and $j$. Define

$$\mathcal{C}_i = \{j : (i,j) \in \mathcal{C}, i < j\} \quad (2)$$

as the set of all nodes that are connected "downstream" from node $i$. The complex power drawn by the load at node $i$ is denoted as $p_i + jq_i$, whereas $P_{ij}$ and $Q_{ij}$ are the active and reactive power flowing from node $i$ toward node $j \in \mathcal{C}_i$ through the connecting branch $(i,j)$. The impedance of that branch is $z_{ij} = r_{ij} + jx_{ij}$.

The load at each node has been modelled as voltage dependent

$$p_i + jq_i = p_i^0\Big(\frac{V_i}{V_i^0}\Big)^{\alpha_i} + jq_i^0\Big(\frac{V_i}{V_i^0}\Big)^{\gamma_i} \quad (3)$$

where $p_i^0$, $q_i^0$ refer to the predisturbance load at node $i$, and $V_i^0$ is the predisturbance voltage magnitude at that node. A load model consisting of a combination of constant power, current, and impedance, commonly referred to as the ZIP model [14],

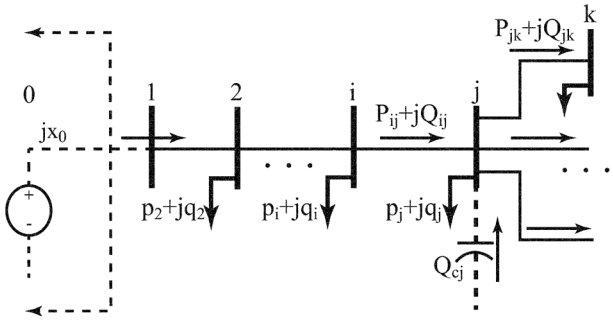


Fig. 3. Radial structure of a distribution feeder.

could just as easily be used though. The reactive power produced by a shunt capacitor $b_i$ at node $i$ is given by $Q_{ci} = b_i V_i^2$. A Thévenin equivalent has been used to model the grid from generation to the feeder source node 1. Source reactance is given by $x_0$, with the source resistance neglected. The Thévenin voltage $V_0$ at node 0 is set to give the desired predisturbance voltage at the feeder source node 1.

It is convenient to model radial feeders of the form shown in Fig. 3 using the *DistFlow* [15] recursive power-flow equations

$$P_{ij} = \sum_{k \in \mathcal{C}_j} P_{jk} + \frac{r_{ij}\left(P_{ij}^2 + Q_{ij}^2\right)}{V_i^2} + p_j \tag{4a}$$

$$Q_{ij} = \sum_{k \in \mathcal{C}_j} Q_{jk} + \frac{x_{ij}\left(P_{ij}^2 + Q_{ij}^2\right)}{V_i^2} + q_j - b_j V_j^2 \tag{4b}$$

$$V_j^2 = V_i^2 - 2\left(r_{ij}P_{ij} + x_{ij}Q_{ij}\right) + \frac{\left(r_{ij}^2 + x_{ij}^2\right)\left(P_{ij}^2 + Q_{ij}^2\right)}{V_i^2} \tag{4c}$$

where $j \in \mathcal{C}_i$. For later use, define

$$\mathbf{P} = \left\{P_{ij} : (i,j) \in \mathcal{C}\right\} \tag{5a}$$

$$\mathbf{Q} = \left\{Q_{ij} : (i,j) \in \mathcal{C}\right\} \tag{5b}$$

$$V = \left\{V_i : i \in \mathcal{N}\right\} \tag{5c}$$

$$p = \left\{p_i : i \in \mathcal{N}\right\} \tag{5d}$$

$$q = \left\{q_i : i \in \mathcal{N}\right\} \tag{5e}$$

$$b = \left\{b_i : i \in \mathcal{N}\right\} \tag{5f}$$

allowing (4) to be written compactly as

$$F(\mathbf{P}, \mathbf{Q}, V, p, q, b) = 0. \tag{6}$$

The load at each node is comprised of both non-PEV base load and PEV-charging load. PEV-charging load is effectively constant (not voltage dependent) under normal operating conditions. This is a consequence of controls that implement a constant current constant voltage (CCCV) charging strategy [16]. Denote by $\beta_i$, the active power drawn by PEV chargers at node $i$ as a fraction of the total predisturbance active power consumption at that node. The power factor of the PEV-charging load[2] is denoted by $pf_i$. Therefore, the PEV load is given by

$$p_{ev,i}(\beta_i) + jq_{ev,i}(\beta_i) = \beta_i p_i^0 \left(1 + j\frac{\sqrt{1 - pf_i^2}}{pf_i}\right) \tag{7}$$

and the predisturbance non-PEV load is given by

$$p_{nev,i}^0(\beta_i) + jq_{nev,i}^0(\beta_i) = (1 - \beta_i)p_i^0 + j\left(q_i^0 - \beta_i p_i^0 \frac{\sqrt{1 - pf_i^2}}{pf_i}\right). \tag{8}$$

Due to the voltage dependence of the non-PEV load, it follows from (3) that the actual postdisturbance demand will be given by

$$p_{nev,i}(V_i, \beta_i) = p_{nev,i}^0(\beta_i)\left(\frac{V_i}{V_i^0}\right)^{\alpha_i} \tag{9a}$$

$$q_{nev,i}(V_i, \beta_i) = q_{nev,i}^0(\beta_i)\left(\frac{V_i}{V_i^0}\right)^{\gamma_i}. \tag{9b}$$

Later formulations will use the notation

$$p_{nev}(V, \beta) = \{p_{nev,i}(V_i, \beta_i); i \in \mathcal{N}\} \tag{10a}$$

$$q_{nev}(V, \beta) = \{q_{nev,i}(V_i, \beta_i); i \in \mathcal{N}\}. \tag{10b}$$

### B. Voltage-Control Assumptions

Based on SAE J2894, PEV chargers are free to trip for voltage sags that last longer than 12 cycles (0.20 s for a 60 Hz system.) It is therefore likely that many PEV chargers will trip in the 0.20–0.25 s time frame. Upon clearing of the initiating disturbance, voltages will rise instantaneously to values that exceed predisturbance conditions. This entire process is fast relative to standard distribution-level voltage controls. The following assumptions are therefore made:

- Distribution transformers and voltage regulators will require at least a few seconds to tap following disturbance clearing [17], though they will eventually operate to restore voltages to an acceptable level. This time delay is necessary to ensure that ambient voltage fluctuations do not cause excessive tapping.
- Shunt capacitors will not trip immediately upon disturbance clearing, though they will switch after some time. Again, a time delay is necessary to prevent excessive switching.

Hence, distribution feeders will be exposed to high voltages for an appreciable period following disturbance clearing.

## IV. Problem Formulation

In the two-bus example considered in Section II, determining the relationship between loss of load and consequent voltage rise involved a two-step process as follows.

[2]It will be assumed in later studies that all PEV-charging loads have a power factor of $pf_i = 0.97$ lagging, which is consistent with [9]. This is not a restrictive assumption though.

Step 1) For a given total load (non-PEV plus PEV), the susceptance $b$ required to achieve the desired predisturbance voltage was determined.

Step 2) With susceptance fixed at the value determined in Step 1), the load reduction required for the postdisturbance voltage to reach the maximum allowable value of 1.1 p.u. was then calculated.

This process is straightforward for the two-bus case, and can be implemented by coupling together two copies of (1), with the predisturbance values for $p$ and $V$ specified in the first equation, and the voltage threshold $V = 1.1$ p.u. specified in the second equation. This results in two equations in two unknown variables, the susceptance $b$ and the reduced load $p_{red}$. The critical proportion of PEV-charging load is then given by $\beta_{crit} = (p - p_{red})/p$. This formulation provides a direct mapping from $p$ to $\beta_{crit}$.

An equivalent mapping is desired for general multi-node networks of the form shown in Fig. 3. Some adaptation of the two-step process is required, with the following subsections describing a generalized approach.

### A. Predisturbance Conditions

In establishing predisturbance conditions, it is assumed that the feeder normally operates with all node voltages within allowable bounds, for example ±2% of nominal [18], and that power losses are minimized. These requirements can be achieved by placing shunt capacitor banks along the feeder. Capacitor placement and sizing strategies have been extensively studied, with both heuristic guidelines [19]–[21] and optimization techniques [15], [22] widely used. The approach suggested in [19] was adopted to place capacitors, with the capacitors sized using an optimization formulation that minimizes line losses,

$$\min_{b} \ \mathcal{L}(\mathbf{P}, \mathbf{Q}, V) = \sum_{(i,j)\in\mathcal{C}} \frac{r_{ij}\left(P_{ij}^2 + Q_{ij}^2\right)}{V_i^2} \tag{11}$$

subject to

$$F(\mathbf{P}, \mathbf{Q}, V, p^0, q^0, b) = 0 \tag{12}$$

$$0.98 \le V_i \le 1.02, \qquad \forall i \in \mathcal{N} \tag{13}$$

where (12) is just the compact form (6) of the power-flow equations, with loads taking their predisturbance values. The voltage bounds may occasionally lead to infeasibility. In such cases they can be relaxed slightly.

Reliable convergence was obtained using the optimization package CVX [23]. CVX solves convex optimization problems, but the objective function (11) and the power-flow equations (12) are nonconvex. Thus an iterative approach was adopted, whereby at each iteration, convex approximations of (11) and (12) were used. At each step a convex optimization was solved, followed by an update of the power-flow variables using (12). This process generally converged in a few iterations.

### B. Postdisturbance Voltage Rise

Under postdisturbance conditions, with some of the PEV load disconnected due to the voltage-sag event, voltages across the distribution feeder will tend to be higher than normal. It is assumed that the status of shunt capacitors does not change during the event, so the values of $b$ obtained from the optimization (11)–(13) will remain fixed. The aim is to determine the smallest loss of PEV-charging load across the feeder that would cause the voltage at any of the nodes to encounter its limiting value of 1.1 p.u. This problem can be addressed using the optimization formulation

$$\min_{\beta} \sum_{i\in\mathcal{N}} \beta_i p_i \tag{14}$$

subject to

$$F\big(\mathbf{P}, \mathbf{Q}, V, p_{nev}(V,\beta), q_{nev}(V,\beta), b\big) = 0 \tag{15}$$

$$\max\{V\} = 1.1 \tag{16}$$

where the non-PEV loads $p_{nev}(V,\beta)$ and $q_{nev}(V,\beta)$ refer to (10).

To overcome the nonconvexity inherent in (16), this maximum-voltage constraint is enforced for a single node voltage at a time, replacing (16) by the constraint $V_i = 1.1$ p.u. for a particular node $i$. This is effective as usually only a few nodes are candidates for the highest voltage. If a node voltage is forced to 1.1 p.u., and that causes other nodes to have higher voltages, then the optimization is repeated with the voltage constraint enforced for the node with the highest voltage. With some prior knowledge of likely high-voltage buses, this procedure generally only needs to be repeated once or twice.

## V. Case Studies

Two distribution feeder examples will be used to illustrate the risk of overvoltages as PEV-charging load increases. The first is a 23 kV feeder that has no lateral branches [24], and the second is the standard IEEE-34 distribution feeder [25], [26].

### A. 23 kV 10-Node Primary Feeder

The feeder data for this example were obtained from [24]. The feeder was modified to include the Thévenin equivalent representation of the grid, in accordance with Fig. 3. Shunt capacitors were placed at nodes 7 and 10 to ensure predisturbance voltages were within allowable bounds of ±2%. All non-PEV demand was modelled as voltage dependent (constant current characteristic) unless otherwise noted.

A typical voltage profile along the feeder is shown in Fig. 4. In producing this particular case, all loads were uniformly scaled up by 25%. It is clear that all voltages are acceptable prior to the loss of PEV-charging load. Fig. 4 also illustrates the rise in voltage that occurs when PEV load is disconnected. For this particular case, 33.2% of the load at every node was tripped. This resulted in the voltage at node 10, which is farthest from the substation, rising to exactly 1.1 p.u.

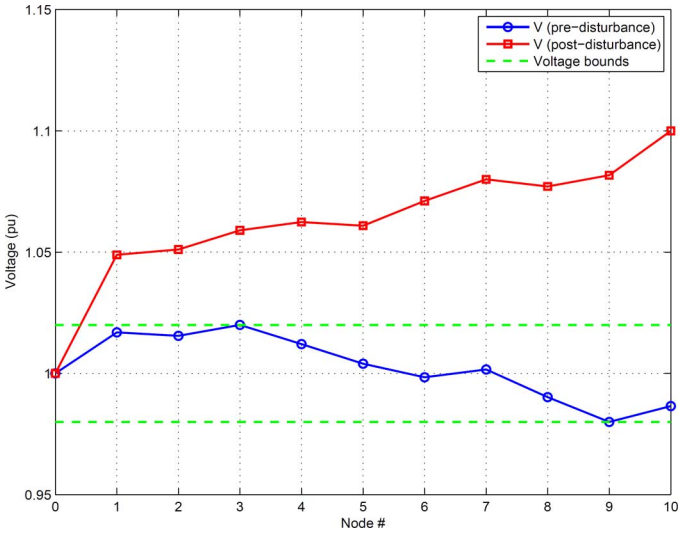


Fig. 4. Predisturbance and postdisturbance voltage profile along the 10-node primary feeder.

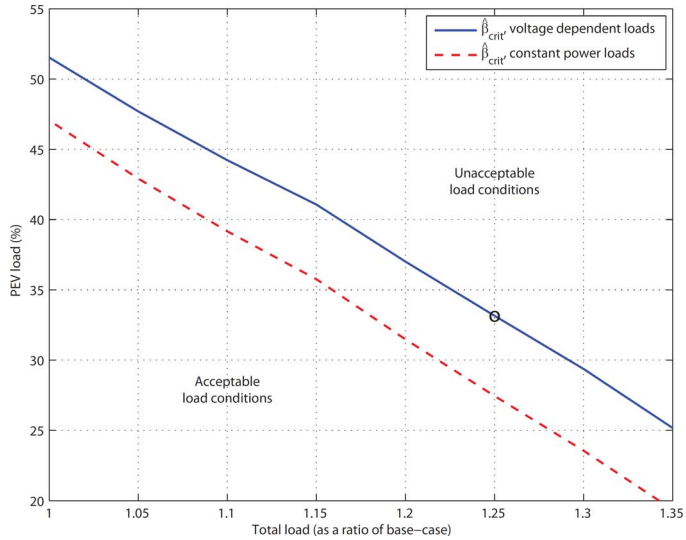


Fig. 5. Allowable PEV load as the total load increases, with $\beta_i$ uniform across the 10-node primary feeder.

This case will initially be used to consider various PEV loading scenarios that help quantify the effects of the spatial distribution of PEVs along a feeder. A probabilistic simulation will then explore the temporal characteristics of PEV charger tripping.

*1) Uniform PEV-charging Load:* For this case, it was assumed that the PEV-charging load was spread uniformly across the feeder, such that the PEV load fraction $\beta_i$ was the same for every node. By setting $\beta_i = \hat{\beta}, \forall i \in \mathcal{N}$, the constraints (15)–(16) form a set of equations that has dimension equal to the number of variables. As a result, direct solution yields the critical value $\hat{\beta}_{crit}$ that corresponds to $\max(V) = 1.1$ p.u.[3] This value separates acceptable cases ($\hat{\beta} < \hat{\beta}_{crit}$) from unacceptable situations ($\hat{\beta} > \hat{\beta}_{crit}$).

To explore different loading scenarios, the total load on the feeder was scaled from 100% to 135% of the base-case load data given in [24]. Shunt capacitors were sized using (11)–(13) whenever they were required to improve the predisturbance voltage profile along the feeder. Furthermore, voltage dependence of non-PEV loads was considered by comparing constant-current and constant-power models. The resulting values of $\hat{\beta}_{crit}$ are plotted in Fig. 5, with the solid and dashed lines corresponding to constant-current and constant-power modelling of non-PEV loads, respectively. The voltage profile shown in Fig. 4 corresponds to the point marked "**o**" in Fig. 5.

Any point above the curve describes an unacceptable loading condition, as the postdisturbance voltage of at least one node exceeds 1.1 p.u. Loading conditions below the curve result in acceptable postdisturbance voltages. It may be concluded from Fig. 5 that for high loading levels, the rise in voltage following a disturbance may be excessive even when the PEV-charging load penetration is quite low. Also, voltage dependence of non-PEV loads tends to moderate the postdisturbance rise in voltages. This is because the increase in non-PEV load with voltage partially compensates the reduction in PEV demand.

[3]Constraint switching associated with (16) can be handled in a similar way to that described in Section IV-B.

*2) Sensitivity To Location:* The location of PEV-charging load along a distribution feeder has an important influence on postdisturbance voltage rise. The effect of load loss tends to become magnified as the distance from the substation increases. The relative significance of different locations can be determined through the use of (15)–(16). Consider an investigation of PEV load at two locations, nodes $i$ and $j$. The corresponding values of $\beta_i$ and $\beta_j$ are free variables in (15), while $\beta_k, k \neq i, j$, are fixed for all other nodes. This leads to (15)–(16) having one more variable than constraint. This under-determined set of equations describes a 1-manifold (or curve) which can be obtained using a continuation process [27]. The simplest approach is to assign a series of values to $\beta_i$ and use (15)–(16) to calculate the corresponding values for $\beta_j$. The resulting curve separates acceptable loading conditions (below the curve) from those that would leave the system vulnerable to postdisturbance overvoltages (above the curve).

This procedure was used to compare the relative importance of PEV loads at nodes 6 and 10 in the 10-node feeder. The results are shown in Fig. 6 for two different background loading conditions, 1) all loads were scaled to 125% of their base-case values in [24], and 2) all loads were scaled by 135%. The proportion of PEV-charging load at all nodes other than 6 and 10 was held at $\beta_k = 0.25, k \neq 6, 10$. The relationship between $\beta_6$ and $\beta_{10}$ is very close to affine, with both lines in Fig. 6 having slopes of approximately $-0.33$. This indicates that a change in $\beta_6$ of 0.2 (meaning an extra 20% of the load at node 6 is due to PEV charging) has the same overvoltage outcome as changing $\beta_{10}$ by around $0.33 \times 0.20 = 0.066$. It follows that the load at node 10 has a much more significant influence on the overvoltage phenomenon of interest. Even though the result is to be expected in this case, as node 10 is at the very end of the feeder, this process provides a valuable analysis tool for cases that are not so straightforward.

*3) Maximum Vulnerability:* The optimization formulation (14)–(16) determines the minimum PEV load loss necessary to cause unacceptable postdisturbance voltages. This effectively

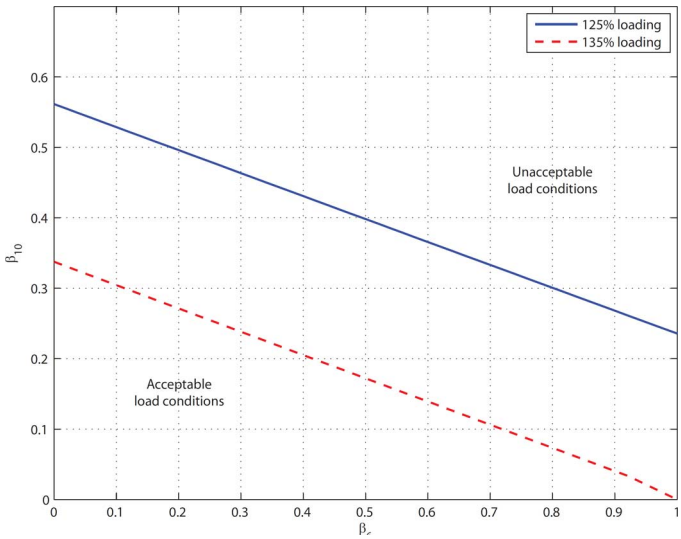


Fig. 6. Sensitivity between $\beta_6$ and $\beta_{10}$ for two loading scenarios on the 10-node primary feeder.

TABLE I
MINIMUM PEV-CHARGING LOAD NECESSARY TO CAUSE UNACCEPTABLE POSTDISTURBANCE VOLTAGES ON THE 10-NODE PRIMARY FEEDER

| $\beta_i$ | | % loading | | | | | | | |
|---|---|---|---|---|---|---|---|---|---|
| | | 100 | 105 | 110 | 115 | 120 | 125 | 130 | 135 |
| Node # | 2 | 0 | 0 | 0 | 0 | 0 | 0 | 0 | 0 |
| | 3 | 0 | 0 | 0 | 0 | 0 | 0 | 0 | 0 |
| | 4 | 0 | 0 | 0 | 0 | 0 | 0 | 0 | 0 |
| | 5 | 0 | 0 | 0 | 0 | 0 | 0 | 0 | 0 |
| | 6 | 0 | 0 | 0 | 0 | 0 | 0 | 0 | 0 |
| | 7 | 0 | 0 | 0 | 0 | 0 | 0 | 0 | 0 |
| | 8 | 0 | 0 | 0 | 0 | 0 | 0 | 0 | 0 |
| | 9 | 0.987 | 0.754 | 0.543 | 0.352 | 0.098 | 0 | 0 | 0 |
| | 10 | 1.0 | 1.0 | 1.0 | 1.0 | 1.0 | 0.938 | 0.835 | 0.720 |
| $\frac{\sum_i \beta_i p_i}{\sum_i p_i}$ | | 0.211 | 0.192 | 0.176 | 0.161 | 0.140 | 0.124 | 0.111 | 0.096 |

establishes the locations where loss of PEV load contributes most to voltage rise. Table I presents the results of this optimization for a range of background loading conditions, from the base-case load profile given in [24] to a 35% increase beyond that base level. In all cases, it can be seen that the network is most vulnerable to overvoltages when PEV load is located near the remote end of the feeder. The proportion of PEV load relative to the total feeder load is given by $\sum_i \beta_i p_i / \sum_i p_i$, with values for the various loading conditions given in the last row of the table. For the 135% loading condition, overvoltage vulnerability occurs when PEV-charging load accounts for only 9.6% of the total load. However problems will only arise if all that load is placed at the end of the feeder.

To explore a more reasonable distribution of PEV load, the optimization problem (14)–(16) was augmented by the additional constraints

$$\beta_i \leq 0.5, \qquad \forall i \in \mathcal{N}. \tag{17}$$

This ensures that no more than 50% of the load at any location can be PEV load. The results of this modified formulation are provided in Table II. It is again clear that the network is more

TABLE II
REPEAT OF TABLE I, SUBJECT TO THE CONSTRAINTS $\beta_i \leq 0.5$

| $\beta_i$ | | % loading | | | | | | |
|---|---|---|---|---|---|---|---|---|
| | | 105 | 110 | 115 | 120 | 125 | 130 | 135 |
| Node # | 2 | 0 | 0 | 0 | 0 | 0 | 0 | 0 |
| | 3 | 0.137 | 0 | 0 | 0 | 0 | 0 | 0 |
| | 4 | 0.5 | 0 | 0 | 0 | 0 | 0 | 0 |
| | 5 | 0.5 | 0.471 | 0.025 | 0 | 0 | 0 | 0 |
| | 6 | 0.5 | 0.5 | 0.5 | 0.173 | 0 | 0 | 0 |
| | 7 | 0.5 | 0.5 | 0.5 | 0.5 | 0.235 | 0 | 0 |
| | 8 | 0.5 | 0.5 | 0.5 | 0.5 | 0.5 | 0.327 | 0 |
| | 9 | 0.5 | 0.5 | 0.5 | 0.5 | 0.5 | 0.5 | 0.498 |
| | 10 | 0.5 | 0.5 | 0.5 | 0.5 | 0.5 | 0.5 | 0.5 |
| $\frac{\sum_i \beta_i p_i}{\sum_i p_i}$ | | 0.397 | 0.310 | 0.252 | 0.206 | 0.167 | 0.136 | 0.106 |

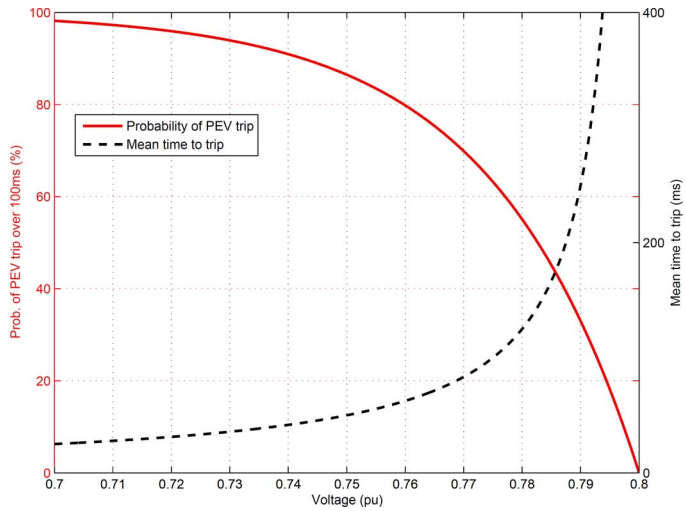


Fig. 7. Probabilistic PEV tripping characteristic.

vulnerable to overvoltages when PEV loads are further from the substation. Based on the scenarios presented in Table II, a relatively small amount of PEV-charging load is required for overvoltage vulnerability. Considering the 125% loading case, for example, unacceptable overvoltages may occur when only 16.7% of the total load is due to PEV charging.

*4) Probabilistic Simulation:* The SAE standard [9] governing the response of PEV chargers to voltage abnormalities specifies that chargers must ride through low voltages for up to 12 cycles (200 ms for 60 Hz systems). However, PEV chargers may trip if voltages remain below 0.8 p.u. The lower the voltage, the more likely tripping becomes. This relationship between voltage and mean time-to-trip can be captured by an exponential probability distribution that is parameterized by voltage. Given a voltage deviation $\Delta V = 0.8 - V > 0$, the probability that a PEV charger trips over a time interval $T$ (ms) is given by the cumulative distribution function,

$$P(\text{PEV trips during } T) = 1 - e^{-\lambda(\Delta V)T} \tag{18}$$

where the rate parameter $\lambda(\Delta V) > 0$ is a function of the voltage dip. The tripping characteristic shown in Fig. 7 was achieved using $\lambda(\Delta V) = 0.4\Delta V$ (1/ms).

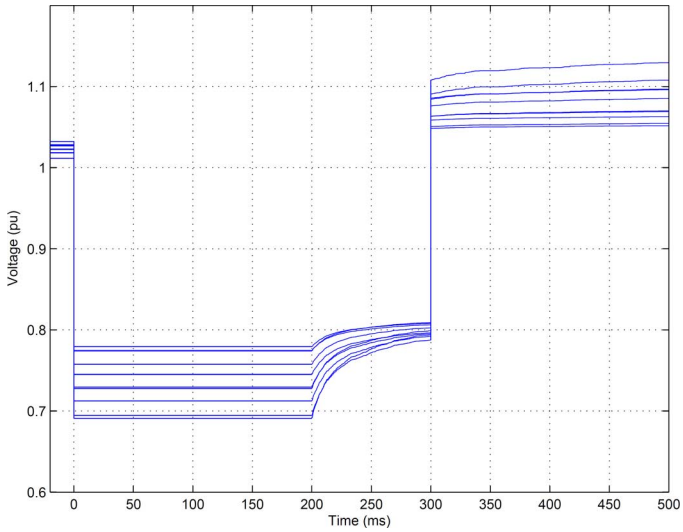


Fig. 8. Response of the voltage at each node to a 300 ms voltage sag on the 10-node primary feeder.

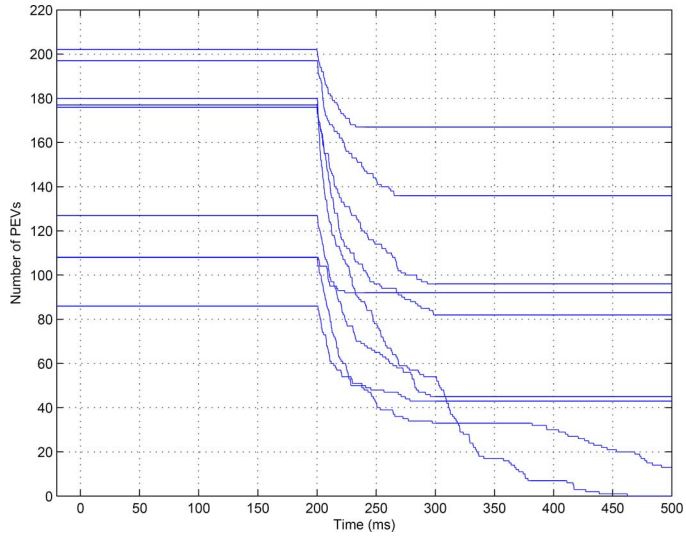


Fig. 9. Number of PEV chargers connected at each node, for a 300 ms voltage sag on the 10-node primary feeder.

Likewise, PEV chargers will trip when exposed to voltages above 1.1 p.u. The probability of such overvoltage tripping can be modelled in a similar way.

For this illustration, it was assumed that chargers accounted for 50% of the load at each node, and that every charger drew 5 kW. It was also assumed that all chargers were governed by the probabilistic tripping characteristic of Fig. 7, with $\Delta V$ for each charger given by the node to which it was connected.

Node 0 was subjected to a voltage drop from 1.0 to 0.8 p.u., for a period of 300 ms. Voltages at all nodes are shown in Fig. 8, while Fig. 9 shows the number of PEV chargers that remain connected at each node. PEVs are prevented from tripping during the first 200 ms, but may trip according to (18) beyond that time. As PEV chargers trip, voltages rise slightly, so the rate of tripping subsides. Nevertheless, once the system voltage is restored to 1.0 p.u. at 300 ms, voltages at some nodes exceed 1.1 p.u. PEV tripping then continues at those nodes due to the excessively high voltages, further exacerbating the overvoltages.

The short-term relationship between the power drawn by a PEV charger and its terminal voltage may depend on many factors, including the charger design and its operating condition (i.e., point on the charging cycle). In order to assess this effect, the load drawn by each charger was modelled according to (3), with the active-power index $\alpha_i$ chosen randomly from the range $\alpha_i \in [0, 2]$, while reactive power was held at a constant power factor (0.97 lagging). A Monte Carlo simulation was undertaken using 1000 randomly chosen sets of PEV-charger load indices. The results are summarized in Fig. 10. It can be seen that voltage dependence of the charging load has only a limited influence on the voltage rise phenomenon. In all cases, the postevent voltage of at least one node exceeded the critical level of 1.1 p.u. The figure also shows that around 50% of the PEV chargers tripped in response to this LV event.

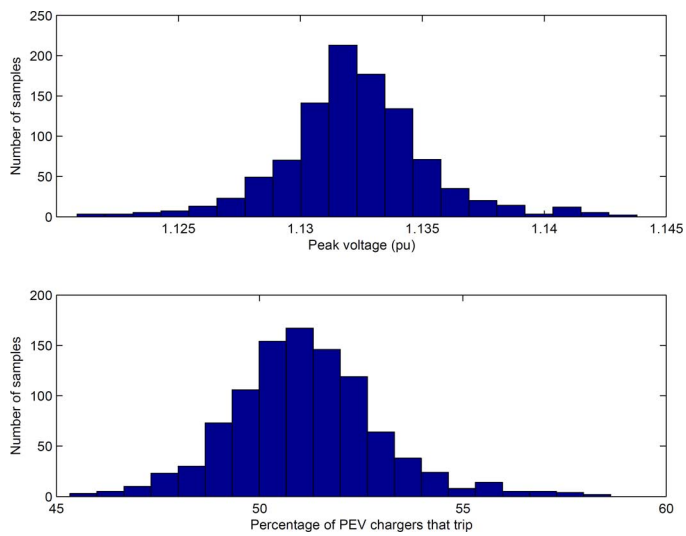


Fig. 10. Results from 1000 simulations, each of the form shown in Figs. 8 and 9. Upper plot: maximum voltage that was observed in each case. Lower plot: percentage of PEV chargers that tripped in each case.

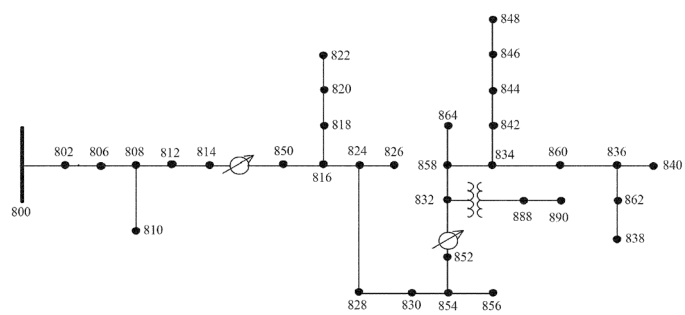


Fig. 11. Standard IEEE-34 distribution feeder.

## B. IEEE-34 Test Feeder

Similar analysis has been undertaken for the standard IEEE-34 distribution feeder [25], [26], which is shown in Fig. 11. This model describes an actual 24.9 kV feeder in Arizona that is long and lightly loaded. PEV-induced overvoltage effects are prominent in this feeder because of its long lines.

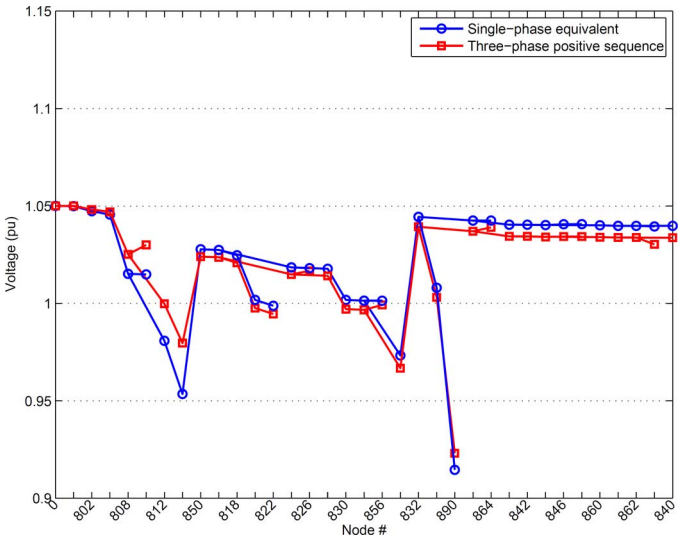


Fig. 12. Comparison between the positive-sequence voltages for the three-phase model and the corresponding voltages for the single-phase equivalent model.

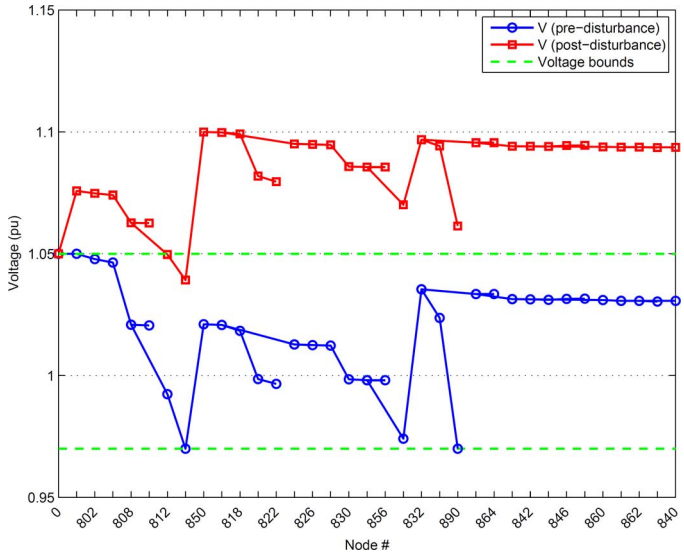


Fig. 13. Predisturbance and postdisturbance voltage profile along the 34-node feeder.

The first step in this investigation was to replicate the three-phase power-flow results given in [26]. Fig. 12 shows the positive sequence voltage profile at the nodes along the feeder. (The lines in the figure indicate physical connections between nodes.) The figure also shows the voltage profile obtained for a single-phase equivalent model. There is generally good agreement, though with some discrepancy around nodes 808–814 due to significant voltage imbalance at those locations.

It is clear from Fig. 12 that some of the node voltages are unacceptably low. To improve the voltage profile, shunt capacitors were added at nodes 822 and 890. Also, a Thévenin equivalent for the higher-voltage grid was incorporated, and the allowable voltage range (13) was relaxed to 0.97–1.05 p.u. The resulting voltage profile is shown in Fig. 13 as the predisturbance case. The investigations reported in Sections V-B1–V-B3 use the single-phase equivalent model. The full three-phase network representation is considered in Section V-B4.

In all cases, non-PEV loads were represented by the ZIP voltage-dependent load model, in accordance with [26].

*1) Uniform PEV-charging Load:* As in Section V-A1, this initial study assumed that PEV-charging load was spread uniformly across the feeder, so $\beta_i = \hat{\beta}, \forall i \in \mathcal{N}$. Fig. 14 shows the variation in the critical value $\hat{\beta}_{crit}$ as the total load on the feeder was decreased from 100% of the base case (given in [26]) to 70% loading. Recall that $\hat{\beta}_{crit}$ corresponds to a postdisturbance voltage profile where $\max\{V\} = 1.1$ p.u. Fig. 13 shows the predisturbance and postdisturbance voltage profiles for the base case (load scaling of 100%) and $\hat{\beta}_{crit} = 0.1988$. This particular case is identified on the curve in Fig. 14 by a "**o**." It should be reiterated that for the base-case loading level, less than 20% of the load needed a trip for a node voltage to reach 1.1 p.u.

*2) Sensitivity to Location:* The continuation process described in Section V-A2 was used to compare the relative importance of PEV loads at nodes 844 and 890, which are on different spurs of the 34-node feeder. The proportion of PEV load at all other nodes was held constant at $\beta_i = 0$. The results

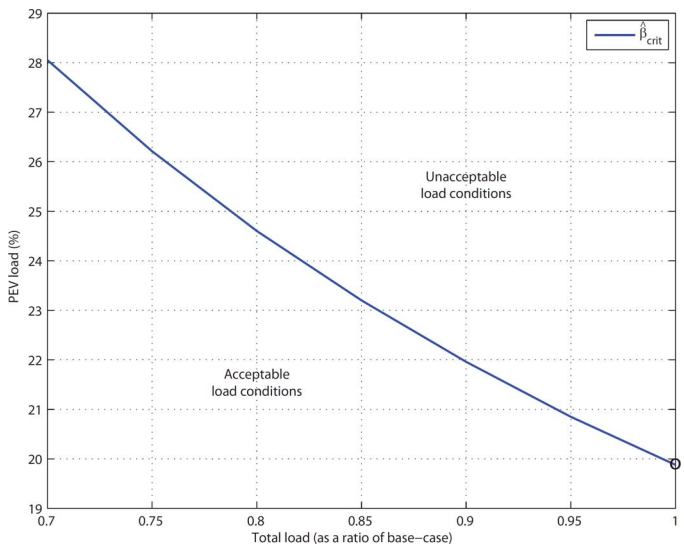


Fig. 14. Allowable PEV load as total load increases, with $\beta_i$ uniform across the 34-node feeder.

for two loading conditions, 70% and 80% of the base case, are presented in Fig. 15. As with the 10-node feeder, the relationship displayed in Fig. 15 is affine over most of the range. In this case, though, the lines have a slope of around $-0.95$. It may be concluded that the PEV load at both locations creates almost the same likelihood of unacceptable postdisturbance voltage rise.

*3) Maximum Vulnerability:* The results of the optimization (14)–(16) coupled with (17), for a range of loading conditions, are presented in Table III. (Only nodes with nonzero entries have been included in the table.) These results identify the locations where high penetration of PEV load makes the network most vulnerable to postdisturbance overvoltages. It is again clear that adding PEV-charging load near the ends of the feeder maximizes vulnerability. For this particular case, the spur associated

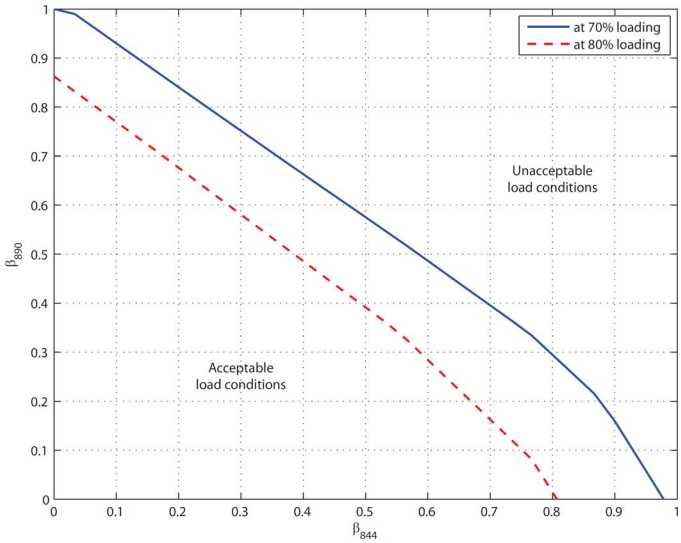


Fig. 15. Sensitivity between $\beta_{844}$ and $\beta_{890}$ for two loading scenarios on the 34-node feeder.

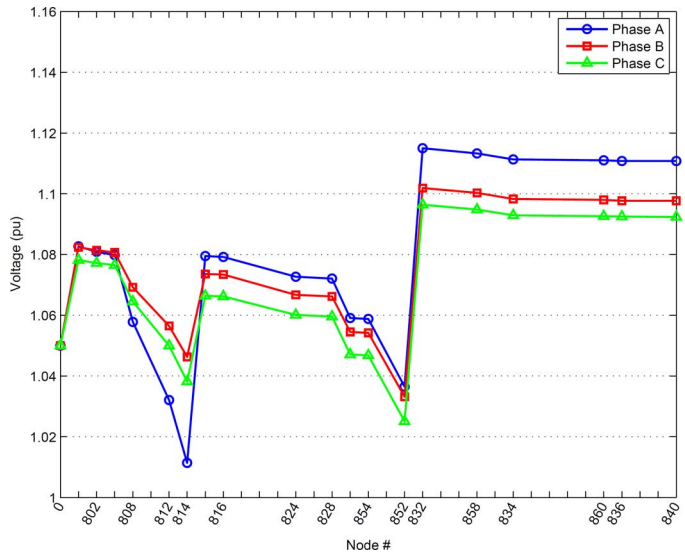


Fig. 16. Postdisturbance phase voltages along the main feeder. Uniform 20% load drop across the three phases for all loads.

TABLE III
MINIMUM PEV-CHARGING LOAD NECESSARY TO CAUSE UNACCEPTABLE POSTDISTURBANCE VOLTAGES ON THE 34-NODE FEEDER. WITH CONSTRAINTS $\beta_i \leq 0.5$

| $\beta_i$ | | % loading | | | | | | |
|---|---|---|---|---|---|---|---|---|
| | | 70 | 75 | 80 | 85 | 90 | 95 | 100 |
| Node | 834 | 0.5 | 0.5 | 0 | 0 | 0 | 0 | 0 |
| | 844 | 0.5 | 0.5 | 0.275 | 0.227 | 0.183 | 0.134 | 0.063 |
| | 890 | 0.381 | 0.319 | 0.5 | 0.5 | 0.5 | 0.5 | 0.5 |
| $\frac{\sum_i \beta_i p_i}{\sum_i p_i}$ | | 0.254 | 0.237 | 0.221 | 0.206 | 0.194 | 0.179 | 0.158 |

with node 890 and the spur off node 834 are most sensitive to PEV load loss.

*4) Overvoltages on the Three-Phase Model:* The previous analysis was undertaken using the single-phase equivalent model. Fig. 14 showed that at 100% loading, a load drop of 20% would result in a node voltage reaching 1.1 p.u. As a comparison, Fig. 16 shows the three phase voltages along the main feeder when a PEV-induced load drop of 20% is applied uniformly across all loads. (For clarity, the voltages on the laterals have not been shown.) The postdisturbance voltage on A-phase at node 832 rises well above 1.1 p.u., while the other phase voltages are close to 1.1 p.u.

If there is imbalance in the distribution of PEV-charging load across the three phases, an even smaller load drop could potentially cause overvoltage issues. Fig. 17 shows the outcome when 30% of the load on A-phase trips but with only 10% of the load on the other phases tripped. (This corresponds to about 17% of the total load on the feeder.) The A-phase voltage rises above 1.1 p.u. from node 832 to the end of the feeder, while the other phase voltages remain within the acceptable range. This example also illustrates that PEV load tripping may lead to significant voltage imbalance.

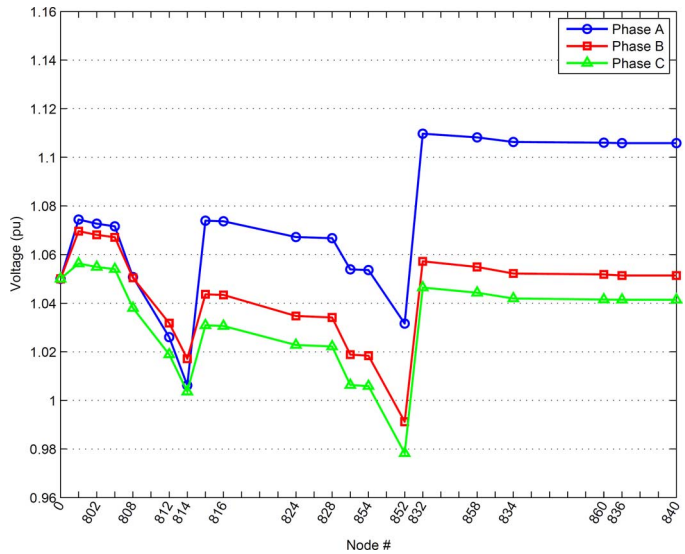


Fig. 17. Postdisturbance phase voltages along the main feeder. Load drop of 30% for all A-phase loads and 10% for loads on the other phases.

## VI. CONCLUSION

The paper has identified a potentially significant issue associated with large-scale PEV charging. When grid voltages sag below 80% of nominal, PEV chargers are likely to trip [9]. Voltage sags often affect entire distribution feeders, and may even be more widespread when initiated by an event on the transmission system. It is therefore quite plausible that voltage-sag events may affect large numbers of PEVs, leading to synchronous response and a consequent drop in load. To put this load drop into context, most PEV charging will occur at night, when non-PEV load is at a minimum. It follows that voltage-sag induced tripping of PEV-charging loads could result in the loss of a significant proportion of the total load.

When the initiating event is cleared, voltages will instantly rise above their predisturbance levels due to the reduction in load. It is shown in the paper, for realistic distribution feeders, that postdisturbance voltages may easily exceed 1.1 p.u. This would result in further load tripping, including many of the

remaining PEV chargers [9]. The resulting overvoltage conditions could damage electrical equipment and remaining loads. The usual methods of controlling distribution feeder voltages, namely, transformer and voltage regulator tapping and capacitor switching, are too slow to prevent overvoltages when the initiating event is cleared.

The underlying load-loss problem is a consequence of the low-voltage characteristics of PEV chargers, which are determined by the governing standard [9]. Altering the standard to ensure grid-friendly low-voltage-ride-through behavior would eliminate widespread PEV load tripping, and postdisturbance overvoltages would become a nonissue.

The paper has shown that potential overvoltage situations can be assessed using tools that are based on the power-flow equations. Three situations have been considered: 1) uniform distribution of PEV-charging load across all loads; 2) sensitivity to charging loads at various locations; and 3) minimum charging load that can cause overvoltage issues. These investigations establish the boundary between benign conditions where postdisturbance voltages remain below 1.1 p.u., and unacceptable situations where at least one node voltage rises above 1.1 p.u.

Two standard distribution test networks have been used to illustrate PEV-induced overvoltage behavior, and to demonstrate the capabilities of the analysis tools. The second of these cases considered the full three-phase feeder representation. It was shown that PEV load tripping could cause excessive voltage imbalance and could result in individual phase voltages rising to unacceptable levels.

## REFERENCES


[1] M. Book, X. Mosquet, G. Sticher, M. Groll, and D. Rizoulis, "The comeback of the electric car? How real, how soon, and what must happen next," Boston Consulting Group, Boston, MA, USA, Focus Rep., Jan. 2009.

[2] R. Lache, D. Galves, and P. Nolan, "Electric cars: Plugged," Global Autos Research Team Deutsche Bank, Jun. 2008.

[3] SAE International, "Electric vehicle and plug in hybrid electric vehicle conductive charge coupler," Surface Vehicle Recommended Practice J1772. Warrendale, PA, USA, Oct. 2012.

[4] C. Fietzek, "Electric vehicle and charging: Charging strategy and communication," presented at the Elect. Power Res. Iinst. Infrastructure Working Council, Tempe, AZ, USA, Dec. 2010.

[5] U.S. Energy Inf. Admin., "2010 electric sales, revenue, and average price: Table 5.a," Washington, DC, USA, Nov. 2011.

[6] Z. Ma, D. Callaway, and I. Hiskens, "Decentralized charging control of large populations of plug-in electric vehicles," *IEEE Trans. Control Syst. Technol.*, vol. 21, no. 1, pp. 67–78, Jan. 2013.

[7] NERC, "Fault-induced delayed voltage recovery," Tech. Ref. Paper, ver. 1.2, Jun. 2009. Princeton, NJ, USA.

[8] D. Kosterev, A. Meklin, J. Undrill, B. Lesieutre, W. Price, D. Chassin, R. Bravo, and S. Yang, "Load modeling in power system studies: Wecc progress update," presented at the IEEE Power Energy Soc. Gen. Meeting, Pittsburgh, PA, USA, Jul. 2008.

[9] SAE International, "Power quality requirements for plug-in electric vehicle chargers," Surface Vehicle Recommended Practice J2894–1. Warrendale, PA, USA, Dec. 2011.

[10] Elect. Power Res. Inst., "EV charging equipment operational recommendations for power quality," Palo Alto, CA, USA, Final Rep. TR-109023, Nov. 1997.

[11] K. Yamashita and O. Sakamoto, "A study on dynamic behavior of load supply system including synchronous generators with and without load drop," presented at the IEEE Power Energy Soc. Gen. Meeting, Minneapolis, MN, USA, Jul. 2010.

[12] G. Price, "A generalized circle diagram approach for global analysis of transmission system performance," *IEEE Trans. Power App. Syst.*, vol. PAS-103, no. 10, pp. 2881–2890, Oct. 1984.

[13] I. Hiskens and R. Davy, "Exploring the power flow solution space boundary," *IEEE Trans. Power Syst.*, vol. 16, no. 3, pp. 389–395, Aug. 2001.

[14] IEEE Task Force, "Standard load models for power flow and dynamic performance simulation," *IEEE Trans. Power Syst.*, vol. 10, no. 3, pp. 1302–1313, Aug. 1995.

[15] M. Baran and F. Wu, "Optimal sizing of capacitors placed on a radial distribution system," *IEEE Trans. Power Del.*, vol. 4, no. 1, pp. 735–743, Jan. 1989.

[16] W. Liu, *Introduction to Hybrid Vehicle System Modeling and Control*. Hoboken, NJ, USA: Wiley, 2013.

[17] C. Colopy, "Step-voltage regulators," in *Electric Power Transformer Engineering*, J. H. Harlow, Ed., 3rd ed. Boca Raton, FL, USA: CRC, 2012, pp. 8.1–8.26.

[18] "Voltage tolerance boundary," Pacific Gas & Electric Company. San Francisco, CA, USA, Jan. 1999.

[19] J. Grainger and S. Lee, "Optimum size and location of shunt capacitors for reduction of losses on distribution feeders," *IEEE Trans. Power App. Syst.*, vol. PAS-100, no. 3, pp. 1105–1118, Mar. 1981.

[20] W. Kersting, *Distribution System Modeling and Analysis*. Boca Raton, FL, USA: CRC, 2002.

[21] H. Willis, *Power Distribution Planning Reference Book*, 2nd ed. Boca Raton, FL, USA: CRC, 2004.

[22] M. Baran and F. Wu, "Optimal capacitor placement on radial distribution systems," *IEEE Trans. Power Del.*, vol. 4, no. 1, pp. 725–734, Jan. 1989.

[23] M. Grant and S. Boyd, CVX: Matlab Software for Disciplined Convex Programming. ver. 1.21, Apr. 2011, Build 808.

[24] J. Grainger and S. Lee, "Capacity release by shunt capacitor placement on distribution feeders: a new voltage-dependent model," *IEEE Trans. Power App. Syst.*, vol. PAS-101, no. 5, pp. 1236–1244, May 1982.

[25] W. Kersting, "Radial distribution test feeders," in *Proc. IEEE Power Eng. Soc. Winter Meeting*, Columbus, OH, USA, Jan. 2001, vol. 2, pp. 908–912.

[26] Distribution System Analysis Subcommittee, IEEE Power and Energy Soc., IEEE 34 node test feeder. Sep. 2010. [Online]. Available: ewh.ieee.org/soc/pes/dsacom/testfeeders/index.html

[27] C. Garcia and W. Zangwill, *Pathways to Solutions, Fixed Points and Equilibria*. Englewood Cliffs, NJ, USA: Prentice-Hall, 1981.


**Soumya Kundu** (M'13) received the B.Tech. (Hons.) degree in electrical engineering and the M.Tech. degree in control systems engineering from the Indian Institute of Technology Kharagpur, India, in 2009, and the Ph.D. degree in control systems from the University of Michigan, Ann Arbor, MI, USA, in 2013.

Currently, he is a Postdoctoral Research Associate at the Center for Nonlinear Studies, Los Alamos National Laboratory, USA. His research interests include integration of renewable generation and plug-in electric vehicles into the electrical grid, demand-side control of power systems, nonlinear control, and nonlinear dynamical systems.

**Ian A. Hiskens** (F'06) received the B.Eng. degree in electrical engineering and the B.App.Sc. degree in mathematics from the Capricornia Institute of Advanced Education, Rockhampton, Australia, in 1980 and 1983, respectively, and the Ph.D. degree in electrical engineering from the University of Newcastle, Newcastle, Australia, in 1991.

He is the Vennema Professor of Engineering in the Department of Electrical Engineering and Computer Science, University of Michigan, Ann Arbor, MI, USA. He has held prior appointments in the Queensland electricity supply industry, and various universities in Australia and the U.S. His research interests lie at the intersection of power system analysis and systems theory. His recent activity has focused largely on integration of renewable generation and controllable loads.

Dr. Hiskens is actively involved in various IEEE societies, and is VP-Finance of the IEEE Systems Council. He is a Fellow of the IEEE, a Fellow of Engineers Australia, and a Chartered Professional Engineer in Australia.